Harnessing TP73-targeted nintedanib: A novel strategy to halt triple-negative breast cancer via p53-PPARα/PI3K-Akt pathway suppression

XIAOMENG ZOU[1,2], SHIYU LI[1], SISI HUANG[1], RUILAN NIU[1], GANG LIU[3] and ZHILI WANG[1]

[1]Department of Ultrasound, The First Medical Center, Chinese People's Liberation Army General Hospital, Beijing 100853, P.R. China; [2]Department of Nephrology, First Medical Center of Chinese People's Liberation Army General Hospital, State Key Laboratory of Kidney Diseases, National Clinical Research Center for Kidney Diseases, Beijing Key Laboratory of Medical Devices and Integrated Traditional Chinese and Western Drug Development for Severe Kidney Diseases, Beijing Key Laboratory of Digital Intelligent Traditional Chinese Medicine for the Prevention and Treatment of Pan-vascular Diseases, Key Disciplines of National Administration of Traditional Chinese Medicine, Beijing 100853, P.R. China; [3]Department of Radiology, The First Medical Center, Chinese People's Liberation Army General Hospital, Beijing 100853, P.R. China

Received April 29, 2025; Accepted July 2, 2025

DOI: 10.3892/ijo.2025.5794

Abstract. Triple-negative breast cancer (TNBC) is an aggressive malignancy with limited treatment options, leading to poor clinical outcomes and the need for novel therapeutic approaches. Nintedanib, a United States Food and Drug Administration-approved multi-kinase inhibitor with anti-fibrotic and anti-angiogenic properties, has shown promise in cancer treatment. However, its precise molecular effects on TNBC have not yet been fully elucidated. Therefore, the present study aimed to investigate the therapeutic potential of nintedanib in TNBC using *in vitro* and *in vivo* models, specifically focusing on its regulatory effects on key oncogenic pathways. The present study utilized TNBC cell lines (MDA-MB-231 and 4T1) and BALB/c mice to evaluate the antitumor efficacy of nintedanib. Cell viability and clonogenic capacity were assessed using Cell Counting Kit-8 and colony formation assays. Subsequently, apoptosis induction and cell cycle progression were determined by flow cytometry, and cell migration and invasion were analyzed through scratch and Transwell assays. To identify underlying mechanisms, potential molecular targets were identified via bioinformatics and network pharmacology, and were validated through western blotting, immunofluorescence and immunohistochemistry. Finally, an orthotopic TNBC mouse model was established and monitored in real time by multimodal ultrasound imaging. The results revealed that nintedanib significantly inhibited TNBC cell proliferation and suppressed stem cell-like properties. Furthermore, it induced cell cycle arrest at the G_2/M phase and promoted apoptosis. Mechanistic analysis revealed that nintedanib activated tumor protein p73 (TP73), leading to the disruption of the p53-peroxisome proliferator-activated receptor α (PPARα)/PI3K-Akt signaling axis. Additionally, it downregulated epithelial-mesenchymal transition (EMT) markers, including Snail and zinc finger E-box-binding homeobox protein 1, thereby mitigating tumor invasiveness. *In vivo*, nintedanib treatment effectively reduced tumor growth, angiogenesis and stiffness, indicating its potential as a viable therapeutic agent for TNBC. In conclusion, nintedanib exerts potent anti-TNBC effects by modulating TP73, disrupting oncogenic signaling via the p53-PPARα/PI3K-Akt axis, and attenuating EMT-associated transcription factors. These findings highlight its potential as a promising targeted therapy for TNBC, warranting further clinical exploration.

Correspondence to: Professor Zhili Wang, Department of Ultrasound, The First Medical Center, Chinese People's Liberation Army General Hospital, 28 Fuxing Road, Beijing 100853, P.R. China
E-mail: wzllg@sina.com

Professor Gang Liu, Department of Radiology, The First Medical Center, Chinese People's Liberation Army General Hospital, 28 Fuxing Road, Beijing 100853, P.R. China
E-mail: 13611245784@126.com

Key words: triple-negative breast cancer, targeted therapy, nintedanib, tumor protein p73, epithelial-mesenchymal transition, apoptosis

Introduction

Breast cancer remains one of the most prevalent malignancies worldwide, with an estimated annual incidence of 2.3 million cases and a continuously escalating burden (1,2). Among its subtypes, triple-negative breast cancer (TNBC) represents 15-20% of all breast cancer diagnoses and is defined by the absence of estrogen receptor (ER), progesterone receptor (PR) and human epidermal growth factor receptor 2 (HER2). This molecular classification contributes to its aggressive nature, high metastatic potential and poor clinical prognosis (3,4). Current TNBC treatment regimens rely on a combination of surgical interventions, chemotherapy and, in some cases,

immunotherapy (5,6). However, these therapeutic options are often hampered by limited efficacy, high recurrence rates and the emergence of drug resistance. Thus, there is a pressing need to identify novel therapeutic strategies that can effectively target TNBC while minimizing adverse effects.

Nintedanib, a United States Food and Drug Administration-approved indolinone-derived multi-kinase inhibitor, is widely used for the treatment of pulmonary diseases, including idiopathic pulmonary fibrosis. It exerts antifibrotic and anti-inflammatory effects primarily by inhibiting receptor tyrosine kinases (RTKs), such as vascular endothelial growth factor receptors (VEGFRs), fibroblast growth factor receptors (FGFRs) and platelet-derived growth factor receptors (PDGFR α/β) (7,8). Previous preclinical and clinical studies have suggested that nintedanib possesses marked antitumor activity across various malignancies, including non-small cell lung cancer, pancreatic cancer and gastric cancer, with ongoing phase II and III clinical trials evaluating its efficacy (9-11). Notably, a phase I clinical trial in patients with early HER2-negative breast cancer demonstrated that the combination of nintedanib and paclitaxel exhibited an acceptable safety profile alongside promising antitumor effects (12). However, the precise molecular mechanisms underlying the anticancer activity of nintedanib in TNBC remain poorly understood.

TNBC is frequently associated with a high prevalence of tumor protein 53 (TP53) mutations, which notably impact tumor progression and therapeutic response (13,14). p53, the gene encoded by TP53, is a tumor suppressor critical in DNA damage repair, apoptosis and cell cycle regulation. Loss of p53 function is a key contributor to chemoresistance, limiting the efficacy of conventional therapies (15,16). Tumor protein p73 (TP73) is a member of the p53 gene family, which can compensate for p53 loss under specific conditions by inducing apoptosis and cell cycle arrest through the transcriptional activation of p53-responsive genes (17-19). Given the pivotal role of TP73 in regulating tumor suppression, pharmacological strategies aimed at activating TP73 may provide a promising approach for targeting p53-deficient TNBC, thereby overcoming resistance to standard treatments.

To the best of our knowledge, the present study is the first comprehensive investigation into the therapeutic potential of nintedanib in TNBC through an integrative bioinformatics and *in vitro* and *in vivo* experiments. The current study focused on the antitumor application of nintedanib in the treatment of TNBC and clarified the underlying mechanism. The findings indicated that nintedanib could serve as a promising targeted therapy for TNBC.

Materials and methods

Cell lines and animal models. TNBC cell lines, MDA-MB-231 and 4T1, were originally sourced from the American Type Culture Collection. The cells were cultured in Dulbecco's Modified Eagle's Medium (Gibco; Thermo Fisher Scientific, Inc.) supplemented with 10-12% fetal bovine serum (FBS; Gibco; Thermo Fisher Scientific, Inc.) under standard conditions of 37˚C in a humidified incubator containing 5% CO_2. A total of 10 female BALB/c mice (age, 4-5 weeks; weight, 20 g) were procured from SPF Biotechnology Co., Ltd. Animals were acclimated for 1 week before the commencement of the study in the animal house at standard conditions of temperature (22±2˚C) and relative humidity of (55±10%). A strict 12-h light/dark cycle was enforced, with lights on at 07:00 a.m. and off at 07:00 p.m., and free access to food and water. The experimental protocols were approved by the Ethics Committee of The First Medical Center, Chinese People's Liberation Army General Hospital (Beijing, China).

Cell viability assay. The cytotoxic effects of nintedanib (MilliporeSigma) were assessed using the Cell Counting Kit-8 (CCK-8; Millipore Sigma). Briefly, 5,000 cells/well were seeded in 96-well plates and incubated overnight for adherence. Cells were subsequently treated with nintedanib at concentrations of 0-20 μM (MDA-MB-231) and 0-4.5 μM (4T1) for 0-72 h under standard conditions of 37˚C. Following treatment, 10 μl CCK-8 reagent was added to each well and incubated for 4 h in the dark. was measured Absorbance at 450 nm using an Elx808 plate reader (Thermo Fisher Scientific, Inc.). The inhibition of cell viability was calculated using the formula: Cell viability (%)=[($A450_{test}$ - $A450_{blank}$)/($A450_{control}$ - $A450_{blank}$)] x 100. All experiments were conducted in triplicate, and half maximal inhibitory concentration (IC_{50}) values were determined via probit regression analysis.

Colony formation assay. Cells were seeded at a density of 500 cells/6-cm culture dish. After a 24-h adherence period, the cells were treated with nintedanib at 0, 3, 5 and 15 μM (MDA-MB-231) or 0, 0.5, 1.5 and 3 μM (4T1) for 4 h under standard conditions of 37˚C. The medium was then replaced with a fresh culture medium and the cells were incubated for 14 days. Colonies were fixed using 4% paraformaldehyde and stained with 0.5% crystal violet (Beyotime Institute of Biotechnology) at room temperature, each for 15 min. After washing with distilled water, colonies that contained >50 cells were counted, and images were captured and analyzed using ImageJ 1.8.0.112 (National Institute of Health). The experiment was repeated three times.

Cell cycle analysis. Cells were treated in 6-well plates ($2.5x10^5$ cells/well) with nintedanib at 5 μM (MDA-MB-231) or 1.5 μM (4T1) for 24 h under standard conditions of 37˚C, harvested, and fixed with 75% ethanol overnight at 4˚C. Approximately $2x10^4$ fixed cells were then treated with RNase at 37˚C for 30 min and stained with propidium iodide (PI; MilliporeSigma) at room temperature for 15 min in the dark before flow cytometric analysis using a FACSAria III flow cytometer (BD Biosciences) running FlowJo software 10.8.1(BD Biosciences). The experiment was conducted in triplicate.

Apoptosis assay. Cells were seeded in 6-well plates ($2.5x10^5$ cells/well) and incubated overnight. After treatment with nintedanib (0, 3, 5 and 15 μM for MDA-MB-231; 0, 0.5, 1.5 and 3 μM for 4T1) for 24 h under standard conditions of 37˚C, apoptosis was assessed using the Annexin V-FITC/PI apoptosis detection kit (Beijing 4A Biotech Co., Ltd.) at room temperature in the dark for 30 min, followed by flow cytometry using a FACSAria III flow cytometer running FlowJo software. All experiments were performed in triplicate.

Wound-healing assay. Cell motility was assessed using a wound-healing assay. In a 6-well plate, monolayers of TNBC cells reaching 90% confluence were scratched with a sterile 1-ml pipette tip, followed by treatment with nintedanib (0, 3 and 6 μM for MDA-MB-231; 0, 0.5 and 1 μM for 4T1) for 0-48 h. Images of cell migration were captured under a light microscope (Olympus Corporation) at 0, 24 and 48 h post-scratch. Cell migration rate was quantified by assessing wound closure percentage. Briefly, the initial scratch area (A_0) was measured immediately after wound generation (t=0). After 24-48 h of treatment, the residual scratch area (A_t) was measured. The migration rate was calculated as the percentage reduction in scratch area using the formula: Wound width (%)=[(A_0 - A_t /A_0] x 100. The migration distance was measured and analyzed by ImageJ 1.8.0.112, and the assays was performed in triplicate.

Transwell migration and invasion assays. Cell migration and invasion were determined using 12-well Transwell chamber inserts (diameter, 6.5 mm; pore size, 8.0 μm; Corning, Inc.). Cells were pre-treated with nintedanib (0, 3 and 6 μM for MDA-MB-231; 0, 0.5 and 1 μM for 4T1) for 24 h and were then seeded in serum-free medium ($5x10^4$ cells/well) in the upper chamber. Migration assays were performed using a 10% FBS-enriched medium in the lower chamber. For invasion assays, the upper chamber was coated with 50 μl Matrigel (Beyotime Institute of Biotechnology) under standard conditions of 37˚C for 30 min to 1 h. Following incubation at 37˚C in a 5% CO_2 incubator for 24 h, migrated or invaded cells were stained with 0.5% crystal violet at room temperature for 20 min. The number of imaging fields was used for bright-field microscopy (magnification, x40) and the findings were quantified by ImageJ. The experiment was repeated in triplicate.

RNA samples for sequencing. MDA-MB-231 human breast cancer cells were divided into control (untreated) and 5 μM nintedanib-treated groups. After 24 h of treatment, total RNA was extracted using TRIzol® reagent (cat. no. 15596018CN; Invitrogen; Thermo Fisher Scientific, Inc.). Briefly, cells in 6-well plates were washed twice with PBS. Then, at room temperature, 1 ml TRIzol was added per well for 5 min. At room temperature, 200 μl chloroform (cat. no. 67-66-3; Millipore Sigma) was added per 1 ml of TRIzol, vortexed for 30 sec, and incubated for 3 min. After centrifugation (12,000 x g, 15 min, 4˚C), the aqueous phase was collected. An equal volume of isopropanol (cat. no. 67-63-0; MilliporeSigma) was added, mixed by inversion and incubated for 10 min at room temperature. RNA was pelleted by centrifugation (12,000 x g, 10 min, 4˚C). The pellet was washed with 75% ethanol, air-dried and dissolved in RNase-free water (cat. no. 10977015; Thermo Fisher Scientific, Inc.) RNA concentration, purity, and integrity were assessed by Nanodrop spectrophotometry (Thermo Fisher Scientific, Inc.)

Bioinformatics analysis and target screening. Stranded RNA sequencing libraries were prepared from total RNA using the SMARTer Stranded RNA-Seq Kit (cat. no. 634839; Clontech; Takara Bio USA, Inc.). After library construction, dsDNA concentration was initially quantified using a Qubit 2.0 Fluorometer (Thermo Fisher Scientific, Inc.). Libraries were then diluted to a working concentration of 1.5 ng/μl in nuclease-free water. Insert size distribution was subsequently assessed with an Agilent 2100 Bioanalyzer (Agilent Technologies, Inc.) using the High Sensitivity DNA chip. Upon confirmation of expected insert size profiles (250-500 bp), the effective library concentration (molar concentration of adapter-ligated fragments) was precisely determined by quantitative PCR. Only libraries exhibiting effective concentrations >1.5 nM were processed for sequencing to ensure data quality. RNA sequencing was performed using the Illumina NovaSeq 6000 platform (Illumina, Inc.) at Novogene Biotechnology Co., Ltd. Novogene Biotechnology Co., Ltd. performed comprehensive RNA sequencing services in strict adherence to the standardized workflows of Illumina, Inc. Starting with 1 μg total RNA input, polyadenylated mRNA was isolated through polyA selection using oligo(dT) magnetic beads (TruSeq™ RNA Sample Prep Kit; Illumina, Inc.), followed by fragmentation in divalent cation-based buffer at 94˚C for 8 min. Double-stranded cDNA synthesis was subsequently conducted with random hexamer primers (Illumina, Inc.) and SuperScript™ II Reverse Transcriptase (Invitrogen; Thermo Fisher Scientific, Inc.). The resulting cDNA underwent systematic library preparation involving three sequential enzymatic treatments: i) End-repair/5'-phosphorylation, ii) 3'-dA-tailing, and iii) Illumina adapter ligation. Libraries were then size-fractionated targeting 300 bp inserts via 2% low-range ultra-agarose gel electrophoresis (Bio-Rad Laboratories, Inc.), amplified through 15 PCR cycles with Phusion High-Fidelity DNA Polymerase (New England BioLabs, Inc.), quantified fluorometrically using a Qubit 2.0 Fluorometer (Thermo Fisher Scientific, Inc.), and finally subjected to paired-end sequencing (2x150 bp) on the Illumina NovaSeq 6000 platform. Principal component analysis (PCA) was employed to assess inter-group heterogeneity and intra-group sample consistency. PCA, a dimensionality reduction technique grounded in linear algebra (specifically, eigenvalue decomposition of the covariance/correlation matrix), extracts principal components capturing the maximum variance within high-dimensional data. This analysis was applied to the gene expression profiles of all samples, quantified as Fragments Per Kilobase of transcript per Million mapped reads (FPKM) values. Differential gene expression between the control and nintedanib-treated groups was analyzed using the DESeq2 R package (https://www.bioconductor.org/packages/release/bioc/html/DESeq2.html), with an adjusted $P \leq 0.05$ and $|\log_2(\text{fold change})| \geq 1$. Volcano plots and heatmaps visualizing the differentially expressed genes (DEGs) were generated using the ggplot 2 3.5.2 (https://ggplot2.tidyverse.org/) and pheatmap 1.0.13 (https://www.rdocumentation.org/packages/pheatmap/versions/1.0.13/topics/pheatmap) packages in R package, respectively. Gene Ontology (GO) enrichment analysis of DEGs was performed using the clusterProfiler package version 3.8.1 in R package (https://www.bioconductor.org/packages/release/bioc/html/clusterProfiler.html), incorporating correction for gene length bias. GO terms with an adjusted P-value <0.05 were considered significantly enriched by the DEGs. Kyoto Encyclopedia of Genes and Genomes (KEGG) is a database resource used to understand high-level functions and utilities of biological systems from molecular-level information, particularly large-scale molecular datasets generated by genome sequencing and other

high-throughput experimental technologies. Statistical enrichment of DEGs within KEGG pathways was also analyzed using the clusterProfiler package 3.8.1.

The molecular structure of nintedanib was retrieved from PubChem (https://pubchem.ncbi.nlm.nih.gov/), converted to Protein Data Bank (PDB) (https://www1.rcsb.org/) format using Open Babel 2.3.2 (https://github.com/openbabel/openbabel/tree/master/tools), and docked to receptor proteins from the PDB. Potential drug targets were predicted using the PharmMapper database (20,21) and cross-referenced with RNA sequencing results using Venny (https://bioinfogp.cnb.csic.es/tools/venny/index.html). Molecular docking was performed using AutoDock Vina 1.1.2 (https://github.com/ccsb-scripps/AutoDock-Vina), with results visualized via PyMOL (https://pymol.org/).

Western blotting. After treatment with nintedanib (0, 3, 5 and 15 μM for MDA-MB-231; 0, 0.5, 1.5 and 3 μM for 4T1) for 24 h under standard conditions of 37˚C, TNBC cells were lysed using radioimmunoprecipitation assay buffer (Beyotime Institute of Biotechnology) supplemented with phosphatase inhibitors and PMSF (100:10:1; Beyotime Institute of Biotechnology). After centrifugation at 12,000 x g for 15 min at 4˚C, protein concentration was quantified using a bicinchoninic acid assay. Subsequently, 30 μg total proteins/lane were loaded in 1X Laemmli buffer (Bio-Rad Laboratories, Inc.) and were then separated by SDS-PAGE on 8-15% gels (Beijing Solarbio Science & Technology Co., Ltd.). Post-transfer, nitrocellulose membranes were blocked with 5% (w/v) non-fat dry milk for 1 h at room temperature with orbital shaking. At 4˚C overnight with gentle agitation, the membranes were incubated overnight at 4˚C with the following primary antibodies in 5% bovine serum albumin (BSA; Beyotime Institute of Biotechnology): Snail Rabbit monoclonal antibody (mAb) (cat. no. 3879T), Slug Rabbit mAb (cat. no. 9585T) and phosphorylated (p)-PI3K Rabbit mAb (cat. no. 17366T) (all from Cell Signaling Technology, Inc.; diluted 1:1,000), Akt Rabbit polyclonal antibody (pAb) (cat. no. 10176-2-AP), p-Akt Mouse mAb (cat. no. 66444-1-Ig), Bcl-2 Rabbit pAb (cat. no. 12789-1-AP), Bax Rabbit pAb (cat. no. 50599-2-Ig), CD133 Rabbit pAb (cat. no. 18470-1-AP), cell division control protein 2 (CDC2) Rabbit pAb (cat. no. 19532-1-AP), cyclin B1 Rabbit pAb (cat. no. 55004-1-AP), E-cadherin Rabbit pAb (cat. no. 20874-1-AP), mammalian target of rapamycin (mTOR) Mouse mAb (cat. no. 66888-1-Ig), p-mTOR Mouse mAb (cat. no. 67778-1-Ig), N-cadherin Rabbit pAb (cat. no. 22018-1-AP), proliferating cell nuclear antigen (PCNA) Rabbit pAb (cat. no. 10205-2-AP), TP73 Mouse mAb (cat. no. 66990-1-Ig), p53 Rabbit pAb (cat. no. 10442-1-AP), PPARα Mouse mAb (cat. no. 66826-1-Ig), PI3K Rabbit pAb (cat. no. 20584-1-AP), vimentin Rabbit pAb (cat. no. 10366-1-AP), zinc finger E-box-binding homeobox protein (ZEB)1 Rabbit pAb (cat. no. 21544-1-AP), ZEB2 Rabbit pAb (cat. no. 14026-1-AP) and β-actin Mouse mAb (cat. no. 66009-1-Ig) (all from Proteintech Group, Inc.; diluted 1:5,000), followed by incubation with goat anti-rabbit/mouse IgG HRP-conjugated secondary antibodies (1:2,000 dilution in BSA; cat. nos. 7074P2 and 91196S; Cell Signaling Technology, Inc.) for 2 h at room temperature in the dark. Subsequently, the blots were visualized using western ECL Substrate (Bio-Rad Laboratories, Inc.) in the ChemiDoc Go system (Bio-Rad Laboratories, Inc.), and relative protein intensity was semi-quantified using ImageJ software and normalized to β-actin, with protein expression expressed relative to the control group. The experiment was performed in triplicate.

Immunofluorescence staining. Cells were seeded in 6-well plates ($2.5x10^5$ cells/well) and treated with nintedanib at 5 μM (MDA-MB-231) or 1.5 μM (4T1) for 24 h under standard conditions of 37˚C. Following treatment, the cells were fixed with 4% paraformaldehyde and permeabilized with 0.5% Triton X-100 for 10 min at room temperature. Non-specific binding was blocked using 3% BSA (Invitrogen; Thermo Fisher Scientific, Inc.) for 1 h at room temperature, and the cells were then incubated overnight at 4˚C with primary antibodies against E-cadherin (1:500; cat. no. GB12083-100; Wuhan Servicebio Technology Co., Ltd.) and N-cadherin (1:500; cat. no. GB12135-100; Wuhan Servicebio Technology Co., Ltd.) at 4˚C overnight. After washing in PBS, the Alexa Fluor® 488-conjugated secondary antibody (1:500; cat. no. GB25301; Wuhan Servicebio Technology Co., Ltd.) was applied for 1 h at room temperature in the dark. Finally, nuclei were counterstained with DAPI (Abcam) in anti-fade mounting medium prior to fluorescence microscopy imaging.

In vivo TNBC model and treatment. The ultrasound system was used to visualize the nipple and mammary fat pad (MFP) of the mice to determine the injection site. Under ultrasound guidance, a 29G syringe needle was horizontally positioned at the fourth left nipple and inserted percutaneously into the MFP. While under ultrasound monitoring, 100 μl ($1x10^7$/ml) 4T1 tumor cell suspension was slowly injected, followed by needle rotation upon withdrawal. After the tumors reached ~50 mm^3, the mice were randomly assigned to the control (PBS dissolved in 3% dimethyl sulfoxide; Millipore Sigma) or nintedanib groups (1 mg/kg, tail vein injection) every 2 days for 2 weeks. Tumor growth was monitored using multimodal ultrasound imaging. On day 15, the animals were sacrificed. If the tumor reached a diameter of 1.5 cm in any direction, or the animal showed any notable signs of pain before reaching this size, humane euthanasia was immediately carried out (150 mg/kg pentobarbital sodium, intraperitoneal injection).

Histological and immunohistochemical analyses. After confirming that the mice had lost consciousness, stopped breathing, their hearts had stopped beating and corneal reflexes were lost, the tumors and major organs were collected, fixed in formalin at room temperature for ≤24 h, embedded in paraffin and sectioned (5 μm). Sections were stained with 1% hematoxylin for 5 min and counterstained with 1% alcoholic eosin for 1 min at room temperature and analyzed via optical microscopy.

For immunohistochemistry, the paraffin-embedded sections were deparaffinized in xylene and rehydrated through graded ethanol. Antigen retrieval was performed in citrate buffer at 98˚C for 20 min. For intracellular epitopes (Ki67/PCNA), permeabilization with 0.1% Triton X-100 (20 min, room temperature) preceded endogenous peroxidase quenching using 3% H_2O_2 (20 min, room temperature). The sections were then blocked with 5% BSA for 1 h at room temperature, then

incubated with the following primary antibodies: Ki67 Rabbit pAb (1:200; cat. no. GB111499-100) and anti-PCNA Rabbit pAb (1:500; cat. no. GB11010-100) (both from Wuhan Servicebio Technology Co., Ltd.) at 4˚C overnight. HRP-conjugated secondary antibodies (1:300; cat. nos. GB23303; Wuhan Servicebio Technology Co., Ltd.) were then applied at 37˚C for 1 h. Subsequently, DAB chromogen (cat. no. G1211; Wuhan Servicebio Technology Co., Ltd.) development was microscopically monitored (1-3 min), followed by hematoxylin counterstaining at room temperature for 5 min. TUNEL assay (cat. no. G1501; Wuhan Servicebio Technology Co., Ltd.) was performed after proteinase K permeabilization (20 μg/ml; 37˚C, 15 min) and followed kit protocols. Images of all slides were captured under light microscopy.

Statistical analysis. GraphPad Prism 4.0 (Dotmatics) was used for statistical analysis. Data are presented as the mean ± SD and the experiments were repeated in triplicate. Comparisons between two groups of tumors volume were made using unpaired Student's t-test, whereas one-way ANOVA was used for multiple comparisons followed by Tukey's post hoc test, with specific focus on comparisons between the group of interest and the control. $P<0.05$ was considered to indicate a statistically significant difference.

Results

Cytotoxicity of nintedanib in TNBC cells. The results of the CCK-8 assay revealed a concentration- and time-dependent decrease in MDA-MB-231 and 4T1 cell viability in response to nintedanib (Fig. 1A and B), suggesting nintedanib may exert cytotoxic effects on TNBC cells. Probit regression analysis revealed that the IC_{50} values of nintedanib at 24, 48 and 72 h were 7.06, 5.0 and 4.39 μM for MDA-MB-231 cells, and 2.12, 1.59 and 1.12 μM for 4T1 cells.

As for antiproliferative effects, colony formation assays showed that nintedanib significantly inhibited the colony-forming ability of TNBC cells (Fig. 1C and D), indicating a suppression of both proliferation and stemness. This was further corroborated by western blot analysis, which demonstrated the downregulation of PCNA, a key marker of cell proliferation, and CD133, a stemness-associated marker, following nintedanib treatment (Fig. 1E and F).

Dysregulated cell cycle progression is a hallmark of cancer proliferation. Flow cytometric analysis revealed that nintedanib treatment significantly altered cell cycle distribution in both TNBC cell lines. In MDA-MB-231 cells, drug exposure led to a non-significant trend toward decrease in the proportion of cells in G_1 phase, accompanied by a concurrent increase in S phase cells. Conversely, in 4T1 cells, treatment resulted in a significant increase in G_1 phase cells and a corresponding decrease in S phase cells. Notably, both cell lines exhibited a significant prolongation/accumulation of cells in G_2/M phase (Fig. 1G and H). Mechanistically, western blot analysis indicated that nintedanib treatment led to a dose-dependent reduction in the expression of CDC2 and cyclin B1, critical regulators of the G_2 phase, suggesting that nintedanib suppresses TNBC cell viability by disrupting G_2 phase progression (Fig. 1E and F).

Nintedanib induces apoptosis in TNBC cells. To further investigate whether nintedanib can induce apoptosis in TNBC cell lines, flow cytometric analysis was performed, demonstrating a dose-dependent increase in early and late apoptosis in both MDA-MB-231 and 4T1 cells following nintedanib treatment (Fig. 2A and B). Western blot analysis further revealed an upregulation of Bax, a pro-apoptotic protein, and a downregulation of Bcl-2, an anti-apoptotic protein, suggesting that nintedanib may induce apoptosis via the intrinsic mitochondrial apoptotic pathway (Fig. 2C and D).

Nintedanib inhibits cell motility and epithelial-mesenchymal transition (EMT) in TNBC cells. Numerous chemotherapeutic agents not only induce apoptosis but also impair tumor cell motility (22), with nintedanib no exception. The results of wound-healing assays indicated a significant dose- and time-dependent reduction in cell motility compared with control cells, as indicated by a significant increase in wound width (Fig. 3A and B). Similarly, Transwell migration and invasion assays confirmed a marked inhibition of TNBC cell motility following nintedanib treatment (Fig. 3C and D).

EMT serves a pivotal role in cancer metastasis (23). Western blot analysis showed that nintedanib treatment resulted in a dose-dependent decrease in the mesenchymal markers N-cadherin and vimentin, along with an increase in the epithelial marker E-cadherin relative (Fig. 4A and B). Immunofluorescence staining further corroborated these findings, demonstrating an upregulation of E-cadherin and a downregulation of vimentin in nintedanib-treated TNBC cells (Fig. 4C and D). These results suggest that nintedanib suppresses TNBC cell migration and invasion by partially reversing EMT.

Nintedanib activates TP73 expression in TNBC cells. Given that the genomic profile of the MDA-MB-231 cell line closely mimics patient tumor characteristics and is well-established for drug sensitivity assessments, metastasis studies and transcriptomics analyses (24,25), this model was selected to investigate transcriptional regulatory mechanisms in TNBC and to identify novel therapeutic targets. RNA sequencing and network pharmacology analyses were employed to investigate the molecular mechanisms underlying the anti-proliferative and anti-migratory effects of nintedanib. A total of 42.26 G high-quality sequencing data were obtained from six samples. PCA revealed a clear separation between the control and nintedanib-treated groups, accounting for 98.18% of the variance (Fig. 5A), indicating that nintedanib significantly alters the transcriptional landscape of TNBC cells.

Differential expression analysis identified 3,723 DEGs, including 1,317 downregulated and 2,406 upregulated genes (Fig. 5B). Using the volcano plot, the expression heatmap of the top 50 DEGs was obtained (Fig. 5C). GO analysis revealed that these DEGs were enriched in biological processes related to 'DNA replication' and 'DNA metabolic process'; cell components related to 'chromosome', 'chromosome, centromeric region' and 'chromosomal region'; and molecular functions related to 'catalytic activity, acting on DNA' (Fig. 5D). KEGG pathway analysis indicated significant enrichment in cancer-related pathways, including the 'cell

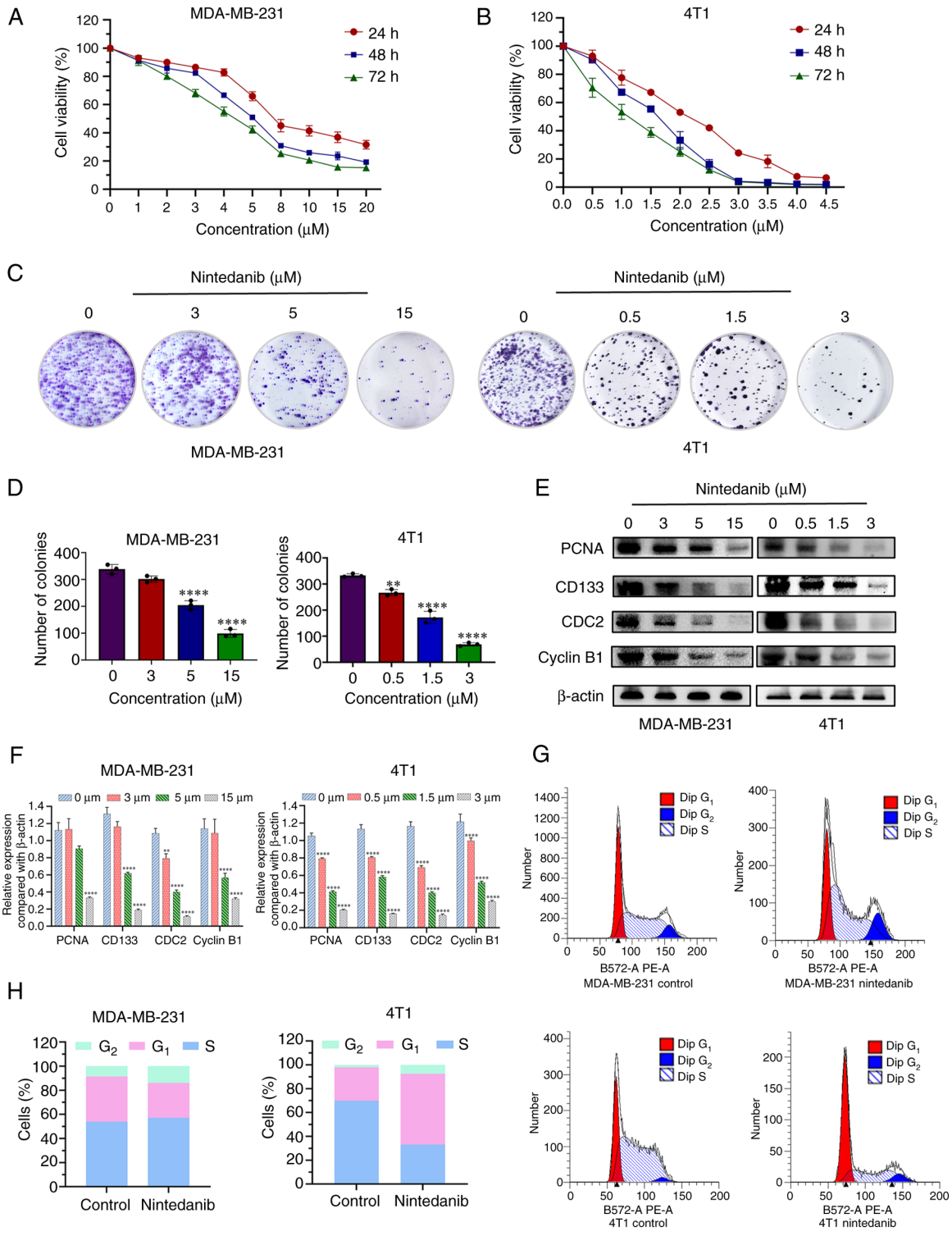

Figure 1. Nintedanib suppresses the viability of triple-negative breast cancer cells. Viability of (A) MDA-MB-231 and (B) 4T1 cells was assessed using the Cell Counting Kit-8 assay following treatment with nintedanib for 24, 48 and 72 h. (C) Colony formation assays were performed to further confirm the inhibitory effects of nintedanib on cell proliferation. (D) Quantification of colony formation rates based on statistical analysis. (E) Western blot analysis of protein expression levels in TNBC cells after nintedanib treatment. (F) Statistical analysis of relative protein expression levels. (G) Cell cycle distribution of MDA-MB-231 and 4T1 cells analyzed after nintedanib treatment by flow cytometry. (H) Quantitative analysis of cell cycle progression. All data are presented as the mean ± SD from three independent experiments. **P<0.01 and ****P<0.0001 vs. control. CDC2, cell division control protein 2; PCNA, proliferating cell nuclear antigen.

cycle', 'cytokine-cytokine receptor interaction', 'JAK-STAT signaling pathway' and 'p53 signaling pathway' (Fig. 5E).

Using PharmMapper, 144 potential targets of nintedanib were identified. A Venn analysis comparing these targets with DEGs identified TP73 as a key overlapping gene (Fig. 5F). Molecular docking analysis revealed a strong binding affinity between nintedanib and TP73, with a binding energy of -5.2 kcal/mol, suggesting that TP73 may

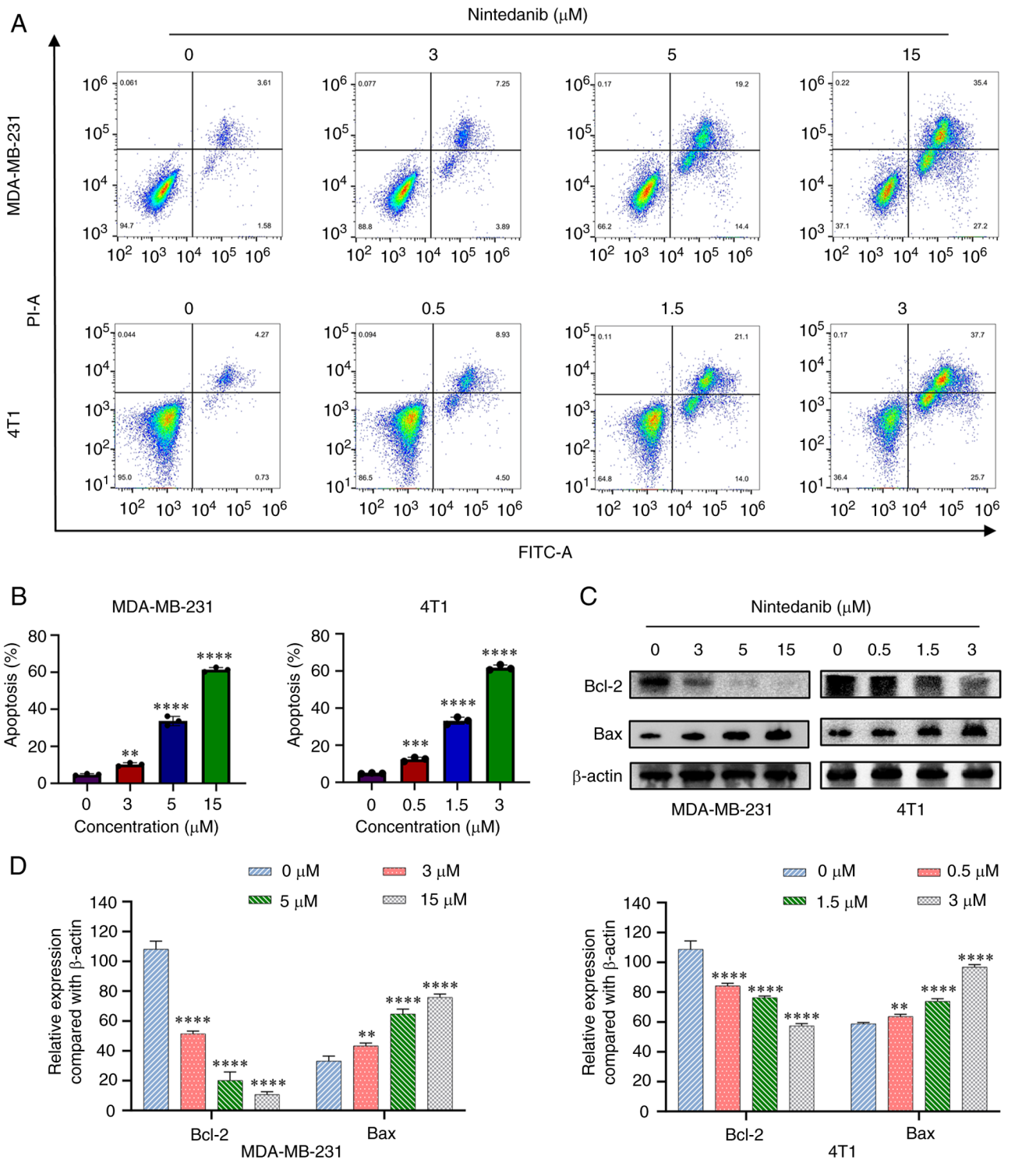

Figure 2. Nintedanib induces apoptosis in TNBC cells. (A) Flow cytometric analysis of apoptosis in TNBC cells following nintedanib treatment. (B) Quantification of apoptosis rates based on flow cytometry data. (C) Western blot analysis of Bcl-2 and Bax protein expression in TNBC cells after nintedanib treatment. (D) Statistical analysis of relative protein expression levels. All data are presented as the mean ± SD from three independent experiments. **P<0.01, ***P<0.001 and ****P<0.0001 vs. control. PI, propidium iodide; TNBC, triple-negative breast cancer.

be a critical target mediating the anticancer effects of nintedanib (Fig. 5G and H).

Nintedanib modulates key signaling pathways in TNBC cells. Based on the transcriptomics analysis, the impact of nintedanib on key signaling pathways was investigated, particularly the p53 and peroxisome proliferator-activated receptor α (PPARα) pathways, using western blotting. Nintedanib treatment significantly upregulated TP73 and p53 expression relative to β-actin, whereas PPARα, p-PI3K, p-Akt and p-mTOR were downregulated in a dose-dependent manner (Fig. 6A and B). Further analyses demonstrated that nintedanib selectively suppressed EMT-transcription factors (EMT-TFs), particularly Snail and ZEB1, while having minimal effects on Slug and

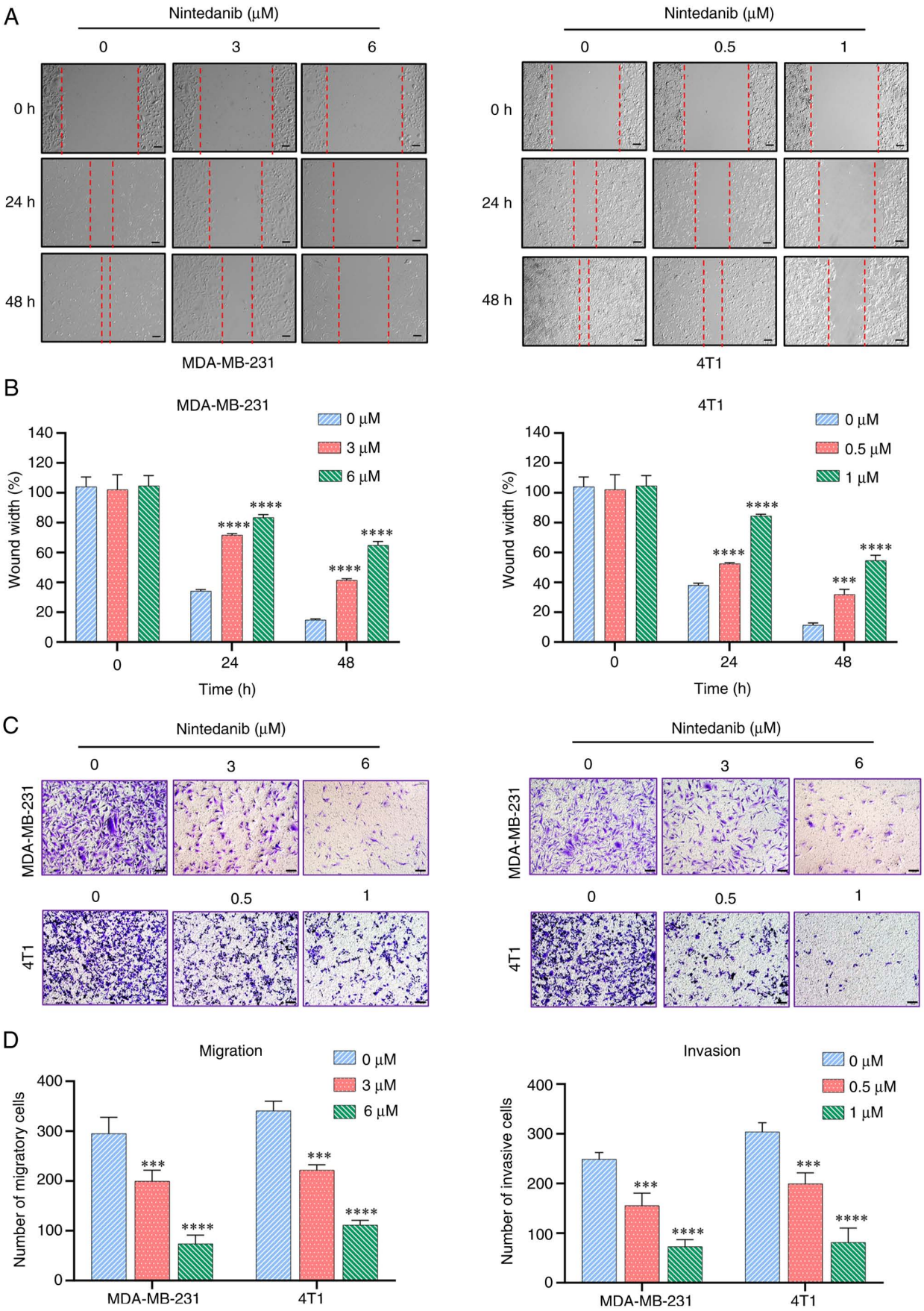

Figure 3. Nintedanib inhibits the migration and invasion of TNBC cells. (A) Wound-healing assays were performed on MDA-MB-231 and 4T1 cells following nintedanib treatment (scale bar, 200 μm). (B) Quantification of relative wound closure rates. (C) Transwell migration and invasion assays were conducted to evaluate the effects of nintedanib on TNBC cell motility (scale bar, 200 μm). (D) Statistical analysis of the number of TNBC cells that migrated or invaded through the membrane. All data are presented as the mean ± SD from three independent experiments. ***P<0.001 and ****P<0.0001 vs. control. TNBC, triple-negative breast cancer.

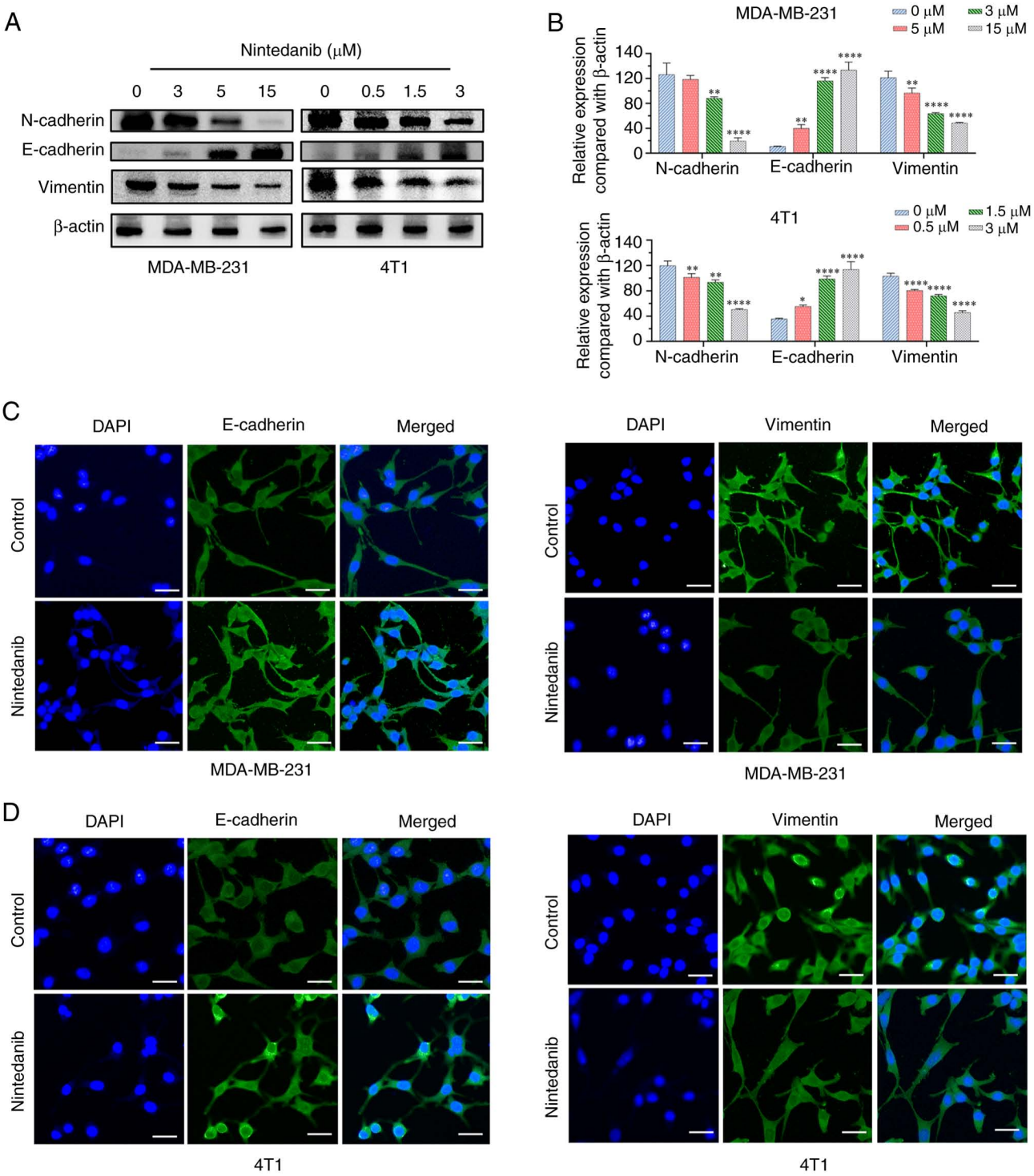

Figure 4. Nintedanib inhibits epithelial-mesenchymal transition in MDA-MB-231 and 4T1 cells. (A) Western blot analysis of N-cadherin, E-cadherin and vimentin expression in TNBC cells following nintedanib treatment. (B) Semi-quantification of relative protein expression levels. Immunofluorescence analysis of E-cadherin and vimentin expression in (C) MDA-MB-231 and (D) 4T1 TNBC cells after nintedanib treatment (scale bar: 50 μm). Data are presented as the mean ± SD from three independent experiments. *P<0.05, **P<0.01 and ****P<0.0001 vs. control. TNBC, triple-negative breast cancer.

ZEB2 (Fig. 6C and D). These findings suggested that nintedanib exerts its inhibitory effects on TNBC by modulating the TP73-p53 and TP73-PPARα pathways and targeting EMT regulators.

Nintedanib suppresses tumor growth in an orthotopic TNBC model. Following ultrasound-guided injection, the orthotopic TNBC model was successfully established in BALB/c mice for the *in vivo* efficacy evaluation of nintedanib (Fig. 7A). Ultrasound-guided imaging was used to monitor tumor progression. On day 14, B-mode tumor imaging revealed the volume was markedly reduced in nintedanib-treated mice compared with controls, color Doppler flow imaging and color power angiography revealed diminished tumor vascularity post-treatment, manifested by reduced density of intratumoral flow

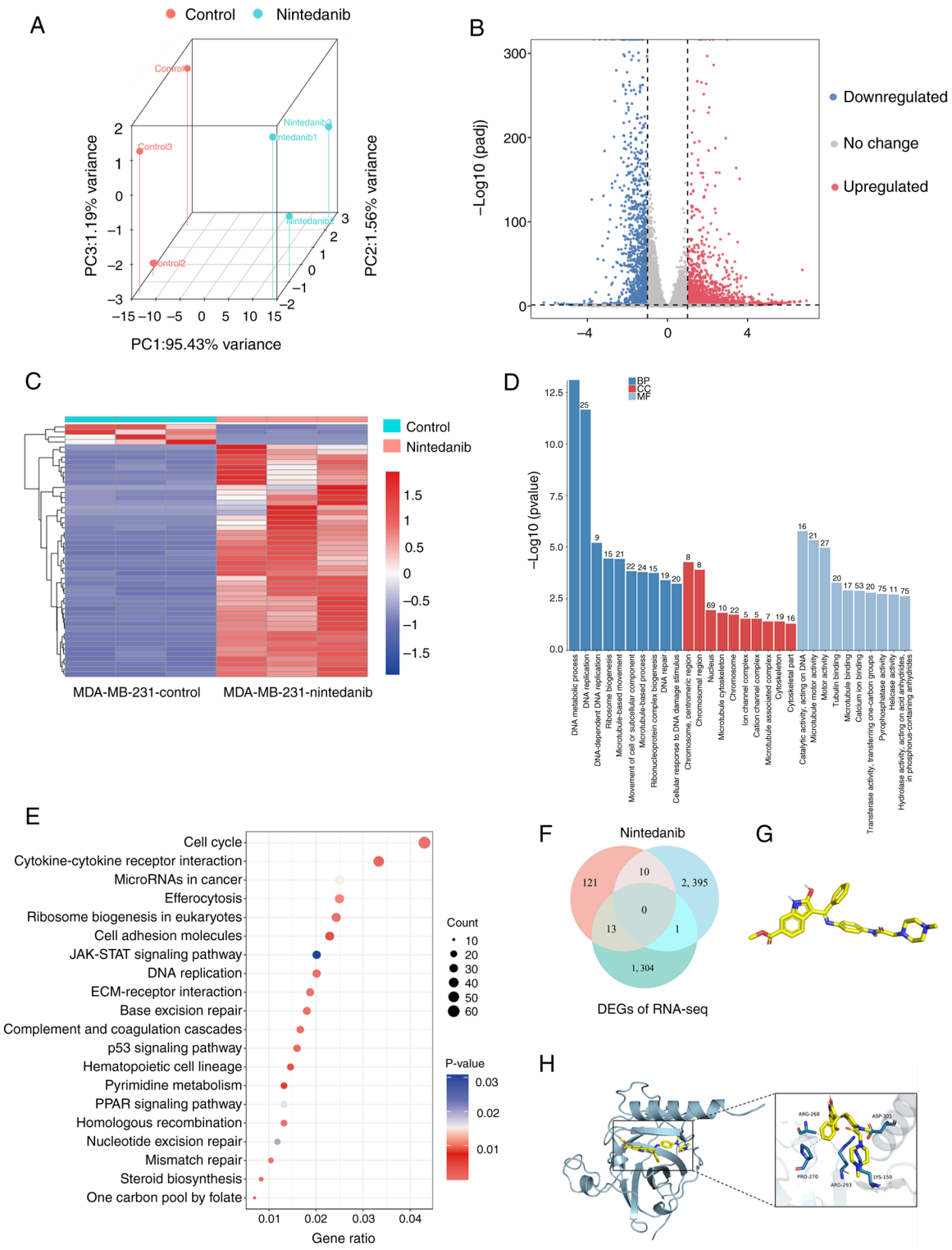

Figure 5. Bioinformatics and network pharmacology analysis of the effects of nintedanib on TNBC. (A) Principal component analysis scatter plot comparing control and nintedanib-treated groups. (B) Volcano plot displaying DEGs identified from RNA-seq data. (C) Heatmap of DEGs across three nintedanib-treated and three control samples, with high expression levels shown in red and low levels in blue. (D) Gene Ontology enrichment analysis of DEGs related to TNBC. (E) Kyoto Encyclopedia of Genes and Genomes pathway analysis of DEGs associated with TNBC. (F) Venn diagram highlighting overlapping genes between DEGs from RNA-seq and nintedanib targets identified via the PharmMapper database. (G) Chemical structure of nintedanib. (H) Molecular docking visualization of the interaction between nintedanib and tumor protein p73. BP, biological process; CC, cellular component; DEGs, differentially expressed genes; MF, molecular function; RNA-seq, RNA sequencing; TNBC, triple-negative breast cancer.

signals and ultrasound strain elastography using fat/muscle as reference tissues indicated significant tissue softening (Fig. 7B and D). During the experiment, the maximum volume of the mouse tumor was 601 mm^3 and the maximum diameter was 1.2 cm. Hematoxylin and eosin staining confirmed the inhibition of angiogenesis (Fig. 7C). Immunohistochemical analysis further demonstrated reduced expression of proliferation markers Ki67

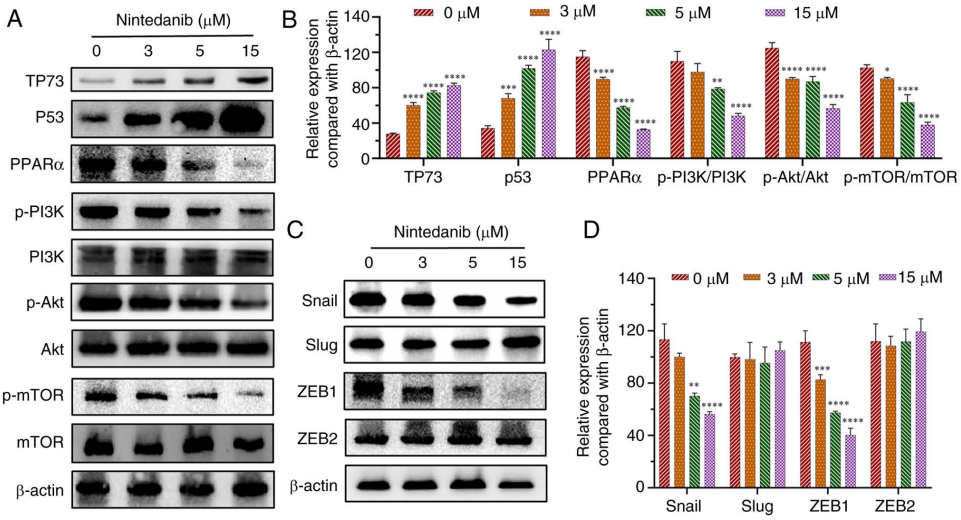

Figure 6. Expression of signaling pathway proteins in TNBC cells following nintedanib treatment. (A) Western blot analysis of key signaling pathway proteins after nintedanib treatment. (B) Semi-quantification of relative protein expression levels. (C) Western blot analysis of EMT regulatory protein expression in TNBC cells after nintedanib treatment. (D) Statistical analysis of relative EMT protein expression levels. All data are presented as the mean ± SD from three independent experiments. *P<0.05, **P<0.01, ***P<0.001 and ****P<0.0001 vs. control. EMT, epithelial-mesenchymal transition; mTOR, mammalian target of rapamycin; p-, phosphorylated; PPARα, peroxisome proliferator-activated receptor α; TNBC, triple-negative breast cancer; TP73, tumor protein p73; ZEB, zinc finger E-box-binding homeobox protein.

and PCNA and increased TUNEL staining, indicating enhanced apoptosis (Fig. 7C).

To assess potential toxicity, body weight was monitored throughout the treatment period, with no significant fluctuations observed (Fig. 7E). Additionally, histological analysis of major organs (heart, liver, spleen, lungs and kidneys) revealed no pathological abnormalities in nintedanib-treated mice (Fig. 7F), suggesting minimal systemic toxicity.

Discussion

TNBC is the most aggressive histological subtype of breast cancer, characterized by the absence of ER, PR and HER2 expression. The absence of well-defined therapeutic targets poses a notable challenge in developing targeted therapies for TNBC. Despite considerable research progress, cytotoxic chemotherapy remains the cornerstone of pharmacological treatment, although its efficacy is limited by suboptimal clinical outcomes and adverse effects (26,27). Among chemotherapeutic agents, doxorubicin (DOX) remains a fundamental treatment option; however, its prolonged use is constrained by the emergence of drug resistance and dose-dependent cardiotoxicity (28). Consequently, drug repurposing strategies have garnered interest in oncology, emphasizing the need for novel, low-toxicity and highly effective tumor-targeted therapies (29). Nintedanib, a multi-targeted tyrosine kinase inhibitor approved for idiopathic pulmonary fibrosis, has demonstrated anti-inflammatory, anti-fibrotic and antitumor properties (30). However, its therapeutic effects on TNBC remain largely unexplored and the present study aimed to address this by systematically investigating the biological effects and molecular mechanisms of nintedanib in TNBC using a combination of bioinformatics, *in vitro* and *in vivo* experimental validation.

The present findings demonstrated that nintedanib significantly inhibits TNBC cell proliferation, stemness and invasion, while inducing apoptosis in a dose-dependent manner. This was confirmed in MDA-MB-231 and 4T1 cell lines by assessing key molecular markers associated with these phenotypic characteristics. Notably, CD133 and PCNA, markers of cancer stemness, exhibited reduced expression upon nintedanib treatment. Similarly, the downregulation of cyclin B1 and CDC2 indicated cell cycle arrest at the G_2 phase, whereas alterations in Bax/Bcl-2 expression confirmed apoptotic induction. Furthermore, EMT markers, including N-cadherin and vimentin, were downregulated, whereas E-cadherin expression was increased, suggesting that nintedanib effectively suppresses the EMT capabilities in TNBC. Ultrasound imaging further validated the *in vivo* efficacy of nintedanib, revealing decreased tumor volume, stiffness index and angiogenesis in treated mice.

Evidence from clinical and preclinical studies has indicated that chronic fibrotic inflammatory diseases and certain drug-resistant malignancies exhibit reduced sensitivity to RTK signaling pathway inhibition (31,32). This observation suggests that, beyond the established effects of nintedanib on classical signaling pathways, compensatory or alternative signaling mechanisms may mediate its inhibitory efficacy in TNBC. To elucidate the underlying mechanism of action, RNA sequencing and molecular docking studies were conducted based on network pharmacology. The results demonstrated that the inhibitory effects of nintedanib on MDA-MB-231 cells were closely associated with TP73 activation. The tumor suppressor TP73 belongs to the p53 family, known for its critical role in maintaining genomic integrity and cellular homeostasis (33,34). While p53 mutations occur in >50% of human cancers, TP73 remains functionally intact in a number of malignancies, retaining its ability to regulate p53 target genes and induce apoptosis. Despite its established significance, the precise regulatory mechanisms of TP73 in TNBC remain poorly understood (35).

Emerging evidence has suggested that TP73 interacts with microRNAs (miRs) to modulate cancer progression.

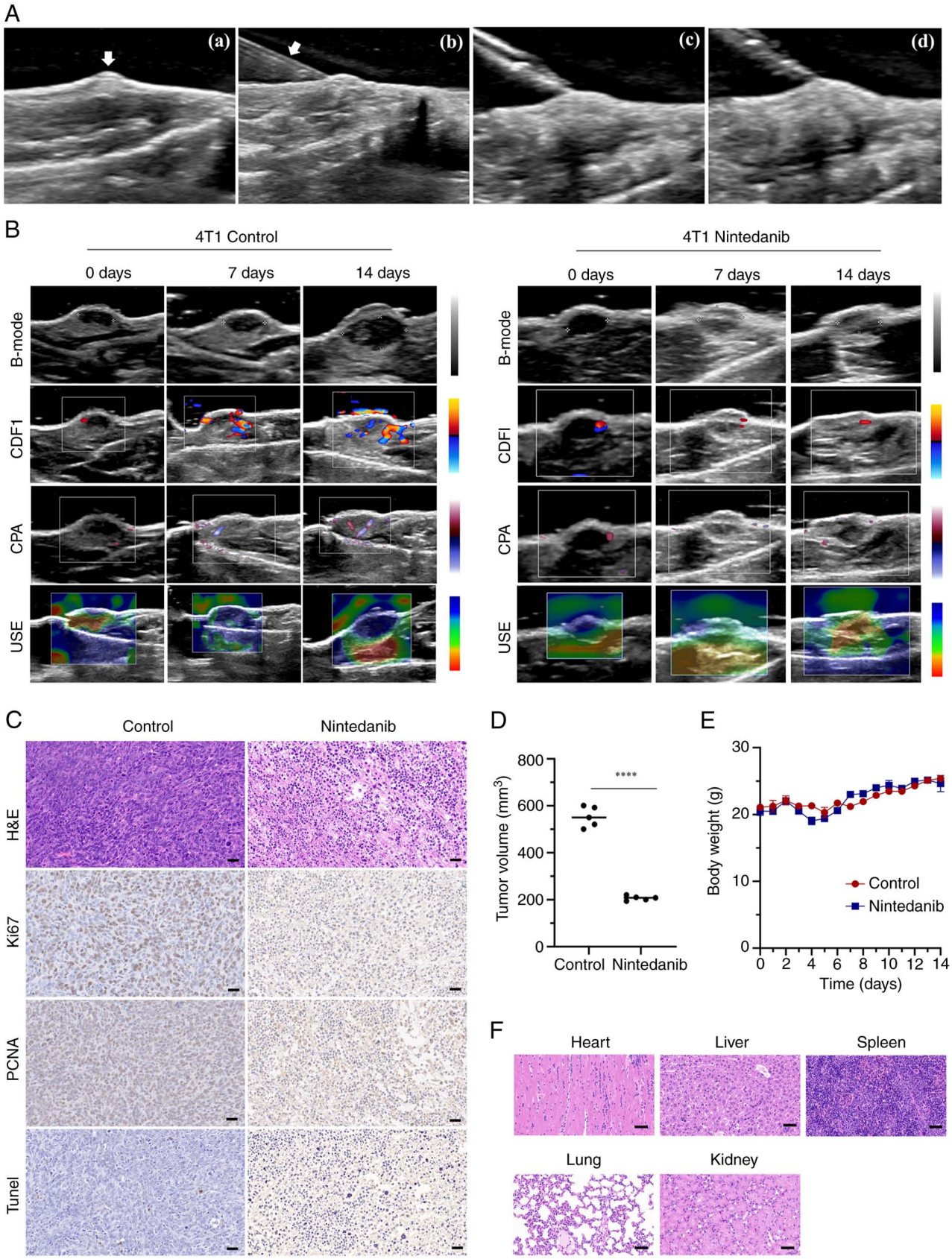

Figure 7. Nintedanib inhibits the growth of 4T1 orthotopic tumors in BALB/c mice. (A) Ultrasound-guided injection of TNBC cell suspension into the MFP: (a) Localization of the mouse MFP before implantation (arrow); (b) needle insertion into the MFP (arrow); (c) injection of the cell suspension into the MFP; (d) needle removal. (B) Multi-modal ultrasound imaging of tumors. (C) Histological analysis of 4T1 orthotopic tumors treated with or without nintedanib, including H&E staining, immunohistochemistry and TUNEL staining (scale bar, 20 μm). (D) Tumor volume measurements following nintedanib treatment. (E) Body weight changes in mice. (F) H&E staining of major organs from TNBC-bearing mice treated with nintedanib (scale bar, 50 μm). All data are presented as the mean ± SD from three independent experiments. ****P<0.0001 vs. control. H&E, hematoxylin and eosin; MFP, mammary fat pad; PCNA, proliferating cell nuclear antigen; TNBC, triple-negative breast cancer; CDFI, color Doppler flow imaging; CPA, color power angiography; USE, ultrasound strain elastography.

Sampath *et al* (36) first reported that in chronic lymphocytic leukemia, TP73 accumulation transcriptionally activates the apoptosis regulator p53 up-regulated modulator of apoptosis, thereby triggering mitochondrial dysfunction, caspase-9 processing and ultimately apoptotic cell death; this positions TP73 as a pivotal nexus bridging epigenetic regulation to apoptotic execution, offering a promising p53-independent therapeutic strategy against malignant cells. Furthermore, TP73 regulates autophagy by transcriptionally activating Atg5, a key autophagy-related gene, further reinforcing its role in cellular homeostasis (37). Given the paucity of research on TP73 in TNBC, the current study provided novel insights by demonstrating that nintedanib significantly upregulates TP73 protein expression in a concentration-dependent manner, consequently inducing TNBC cell apoptosis.

The PI3K-Akt and mTOR signaling pathways are frequently hyperactivated in breast cancer and are crucial mediators of tumorigenesis (38). Prior research has established a functional crosstalk between TP73 and mTOR signaling in ER-positive breast cancer, where rapamycin potentiates tamoxifen efficacy via TP73 induction (39). The present KEGG enrichment analysis of RNA sequencing data suggested that nintedanib may downregulate the PPARα and p53 pathways. Therefore, it was hypothesized that nintedanib may exert its antitumor effects by downregulating the PPARα and PI3K-Akt-mTOR pathways through TP73 activation. Western blot analyses corroborated these findings, showing a dose-dependent decrease in p-mTOR, p-PI3K, p-Akt and PPARα levels upon nintedanib treatment. These results provide compelling evidence that TP73 activation may serve as a key regulatory mechanism underlying the suppressive effects of nintedanib on TNBC progression. Consequently, the present study repositioned nintedanib as a modulator of the TP73-p53-PPARα/PI3K-Akt axis, revealing a novel metabolic regulatory mechanism that extends beyond its canonical RTK inhibitory activity. This finding elucidates the therapeutic efficacy of nintedanib in RTK inhibitor-resistant contexts. Additionally, TP73 could be proposed as a candidate predictive biomarker for therapeutic response in TNBC. Furthermore, a dose-dependent upregulation of TP73 and p53 proteins was detected in respones to nintedanib; it may be proposed that this phenomenon results from p53 protein-function dissociation. MDA-MB-231 cells carry a TP53 R280K mutation that: i) Abrogates apoptosis induction and cell cycle arrest capability; and ii) enhances conformational stability promoting mutant protein accumulation. Nintedanib may further elevate this transactivation-defective p53 via degradation inhibition or stability enhancement, mechanisms warranting future investigation. Crucially, western blot analysis detected total p53 without functional context. The present study hypothesized that under p53-deficient conditions, nintedanib-induced apoptosis and cell cycle arrest may primarily derive from TP73 upregulation. As a p53 homolog, TP73 compensates for p53 loss by activating shared tumor-suppressive targets (e.g., pro-apoptotic genes/CDK inhibitors). Elevated mutant p53 in the present study thus represents a concomitant event rather than the primary therapeutic effector.

TP73 is also implicated in modulating EMT, a fundamental process in cancer metastasis and therapy resistance. Lu *et al* (40) demonstrated that TP73 suppresses EMT in breast cancer cells through regulation of miR-200a/b expression, consequently inhibiting metastatic progression. Similarly, in pancreatic cancer models, TAp73, a subtype of TP73, enhances tumor suppression by promoting canonical TGF-β/Smad signaling while inhibiting non-canonical ERK1/2-mediated pathways (35). The present study indicated that nintedanib treatment can significantly reduce N-cadherin and vimentin levels, while increasing E-cadherin expression, confirming its anti-EMT effects. Furthermore, given the involvement of the PPARα and PI3K-Akt pathways in EMT regulation, it may be proposed that TP73 functions as a critical upstream modulator of these pathways in response to nintedanib treatment.

EMT-TFs, including Snail, Slug, ZEB1 and ZEB2, serve pivotal roles in regulating cancer cell proliferation, migration, invasion, apoptosis and therapeutic resistance (41). Notably, ZEB1 and Snail directly suppress miR-200 family members, leading to EMT induction (42). The present results demonstrated that nintedanib treatment could significantly downregulate ZEB1 and Snail expression in a concentration-dependent manner, whereas Slug and ZEB2 levels remained unchanged. This selective modulation suggests that nintedanib could selectively modulate EMT-TFs, highlighting the necessity for tailored therapeutic strategies that account for TNBC molecular heterogeneity.

Previous studies have established nintedanib as a potent anti-angiogenic agent targeting FGFR, VEGFR and PDGFR (43-45). It has been successfully combined with DOX for non-small cell lung cancer treatment by inhibiting tumor-associated angiogenesis (42). Furthermore, Tu *et al* (46) revealed that nintedanib enhances antitumor immunity by promoting immune cell infiltration, augmenting interferon-γ responsiveness, activating MHC class I antigen presentation and stimulating STAT3 phosphorylation. These findings collectively demonstrate the dual mechanism of action of nintedanib, disrupting angiogenesis while directly inhibiting tumor cell proliferation and survival, positioning it as a promising multi-targeted therapeutic agent. While single-target inhibitors offer therapeutic advantages, they are often constrained by compensatory signaling mechanisms within tumors, necessitating multi-targeted approaches such as nintedanib.

Despite the potential antitumor ability of nintedanib, a major challenge in TNBC treatment is the dense extracellular matrix, which restricts drug penetration and bioavailability. To address this limitation, nanoparticle-based drug delivery systems have emerged as a promising strategy (47). These platforms enhance drug retention, accumulation and penetration within tumors, consequently enhancing therapeutic efficacy. Future investigations should focus on the encapsulation of nintedanib in nanoparticle formulations to optimize its pharmacokinetic profile and tumor-targeted delivery efficiency.

In conclusion, the present study, integrating network pharmacology, transcriptomics and biological validation, provided novel insights into the anti-TNBC effects of nintedanib. the findings revealed that nintedanib may exerts its therapeutic effects by targeting TP73, which modulates the downstream p53-mediated PPARα and PI3K-Akt signaling pathways, while inhibiting EMT regulators such as Snail and ZEB1. These findings expand the understanding of the mechanistic action

of nintedanib in TNBC and provide a foundation for future research aimed at improving targeted therapeutic strategies.

Acknowledgements

Not applicable.

Funding

This work was supported by the National Key R&D Program of China (grant no. 2023YFC2414200) and the National Natural Science Foundation of China (grant no. 8237070671).

Availability of data and materials

The RNA sequencing data generated in the present study may be found in the NCBI BioProject database under accession number PRJNA1280776 or at the following URL: https://www.ncbi.nlm.nih.gov/bioproject/?term=PRJNA1280776. The other data generated in the present study may be requested from the corresponding author.

Authors' contributions

XMZ and ZLW designed this research. XMZ and GL contributed to experimental design and data analysis. XMZ, SYL, SSH and RLN performed the experiments. XMZ wrote this manuscript. XMZ, ZLW and GL assisted in reviewing this manuscript to make it clear. ZLW provided financial support. All authors have read and approved the final manuscript.

Ethics approval and consent to participate

The study was approved by the Ethics Committee of The First Medical Center, Chinese People's Liberation Army General Hospital (approval no. 2024-X20-35).

Patient consent for publication

Not applicable.

Competing interests

The authors declare that they have no competing interests.

References

1. Siegel RL, Miller KD and Jemal A: Cancer statistics, 2018. CA Cancer J Clin 68: 7-30, 2018.
2. Nolan E, Lindeman GJ and Visvader JE: Deciphering breast cancer: From biology to the clinic. Cell 186: 1708-1728, 2023.
3. Lehmann BD, Jovanović B, Chen X, Estrada MV, Johnson KN, Shyr Y, Moses HL, Sanders ME and Pietenpol JA: Refinement of triple-negative breast cancer molecular subtypes: Implications for neoadjuvant chemotherapy selection. PLoS One 11: e0157368, 2016.
4. Bianchini G, De Angelis C, Licata L and Gianni L: Treatment landscape of triple-negative breast cancer-expanded options, evolving needs. Nat Rev Clin Oncol 19: 91-113, 2022.
5. Waks AG and Winer EP: Breast cancer treatment: A review. JAMA 321: 288-300, 2019.
6. Loibl S, Poortmans P, Morrow M, Denkert C and Curigliano G: Breast cancer. Lancet 397: 1750-1769, 2021.
7. Cruwys S, Hein P, Humphries B and Black D: Drug discovery and development in idiopathic pulmonary fibrosis: The changing landscape. Drug Discov Today 29: 104207, 2024.
8. Wollin L, Distler JHW, Redente EF, Riches DWH, Stowasser S, Schlenker-Herceg R, Maher TM and Kolb M: Potential of nintedanib in treatment of progressive fibrosing interstitial lung diseases. Eur Respir J 54: 1900161, 2019.
9. Peng M, Deng J and Li X: Clinical advances and challenges in targeting FGF/FGFR signaling in lung cancer. Mol Cancer 23: 256, 2024.
10. Yao H, Ren Y, Wu F, Cao L, Liu J, Yan M and Li X: The discovery of a novel AXL/triple angiokinase inhibitor based on 6-chloro-substituted indolinone and side chain methyl substitution inhibiting pancreatic cancer growth and metastasis. J Med Chem 68: 465-490, 2025.
11. Dong X, Wang L, Wang D, Yu M, Yang XJ and Cai H: Proteomic study on nintedanib in gastric cancer cells. PeerJ 12: e16771, 2024.
12. Quintela-Fandino M, Urruticoechea A, Guerra J, Gil M, Gonzalez-Martin A, Marquez R, Hernandez-Agudo E, Rodriguez-Martin C, Gil-Martin M, Bratos R, *et al*: Phase I clinical trial of nintedanib plus paclitaxel in early HER-2-negative breast cancer (CNIO-BR-01-2010/GEICAM-2010-10 study). British Br J Cancer 111: 1060-1064, 2014.
13. Adams CM, Mitra R, Xiao Y, Michener P, Palazzo J, Chao A, Gour J, Cassel J, Salvino JM and Eischen CM: Targeted MDM2 degradation reveals a new vulnerability for p53-inactivated triple-negative breast cancer. Cancer Discov 13: 1210-1229, 2023.
14. Yu Z, Dong X, Song M, Xu A, He Q, Li H, Ouyang W, Chouchane L and Ma X: Targeting UBR5 inhibits postsurgical breast cancer lung metastases by inducing CDC73 and p53 mediated apoptosis. Int J Cancer 154: 723-737, 2024.
15. Li G, Lin SS, Yu Zl, Wu XH, Liu JW, Tu GH, Liu QY, Tang YL, Jiang QN, Xu JH, *et al*: A PARP1 PROTAC as a novel strategy against PARP inhibitor resistance via promotion of ferroptosis in p53-positive breast cancer. Biochem Pharmacol 206: 115329, 2022.
16. Musa S, Amara N, Selawi A, Wang J, Marchini C, Agbarya A and Mahajna J: Overcoming chemoresistance in cancer: The promise of crizotinib. Cancers (Basel) 16: 2479, 2024.
17. Ramos H, Raimundo L and Saraiva L: p73: From the p53 shadow to a major pharmacological target in anticancer therapy. Pharmacol Res 162: 105245, 2020.
18. Bisso A, Collavin L and Del Sal G: p73 as a pharmaceutical target for cancer therapy. Curr Pharm Des 17: 578-590, 2011.
19. Rozenberg JM, Zvereva S, Dalina A, Blatov I, Zubarev I, Luppov D, Bessmertnyi A, Romanishin A, Alsoulaiman L, Kumeiko V, *et al*: Dual role of p73 in cancer microenvironment and DNA damage response. Cells 10: 3516, 2021.
20. Wang X, Shen Y, Wang S, Li S, Zhang W, Liu X, Lai L, Pei J and Li H: PharmMapper 2017 update: A web server for potential drug target identification with a comprehensive target pharmacophore database. Nucleic Acids Res 45(W1): W356-W60, 2017.
21. Wang Z, Wang HY, Chung CR, Horng JT, Lu JJ and Lee TY: Large-scale mass spectrometry data combined with demographics analysis rapidly predicts methicillin resistance in Staphylococcus aureus. Brief Bioinform 22: bbaa293, 2021.
22. Sui X, Kong N, Ye L, Han W, Zhou J, Zhang Q, He C and Pan H: p38 and JNK MAPK pathways control the balance of apoptosis and autophagy in response to chemotherapeutic agents. Cancer Lett 344: 174-179, 2014.
23. Kiri S and Ryba T: Cancer, metastasis, and the epigenome. Mol Cancer 23: 154, 2024.
24. Teufelsbauer M, Stickler S, Eggerstorfer MT, Hammond DC and Hamilton G: BET-directed PROTACs in triple negative breast cancer cell lines MDA-MB-231 and MDA-MB-436. Breast Cancer Res Treat 208: 89-101, 2024.
25. Pham TH, Park HM, Kim J, Hong JT and Yoon DY: Interleukin-32θ triggers cellular senescence and reduces sensitivity to doxorubicin-mediated cytotoxicity in MDA-MB-231 Cells. Int J Mol Sci 22: 4975, 2021.
26. Hwang SY, Park S and Kwon Y: Recent therapeutic trends and promising targets in triple negative breast cancer. Pharmacol Ther 199: 30-57, 2019.
27. van Dorst DCH, Dobbin SJH, Neves KB, Herrmann J, Herrmann SM, Versmissen J, Mathijssen RHJ, Danser AHJ and Lang NN: Hypertension and prohypertensive antineoplastic therapies in cancer patients. Circ Res 128: 1040-1061, 2021.
28. Li Y, Zhang H, Merkher Y, Chen L, Liu N, Leonov S and Chen Y: Recent advances in therapeutic strategies for triple-negative breast cancer. J Hematol Oncol 15: 121, 2022.

29. Pushpakom S, Iorio F, Eyers PA, Escott KJ, Hopper S, Wells A, Doig A, Guilliams T, Latimer J, McNamee C, *et al*: Drug repurposing: Progress, challenges and recommendations. Nat Rev Drug Discov 18: 41-58, 2019.
30. Pan L, Cheng Y, Yang W, Wu X, Zhu H, Hu M, Zhang Y and Zhang M: Nintedanib ameliorates bleomycin-induced pulmonary fibrosis, inflammation, apoptosis, and oxidative stress by modulating PI3K/Akt/mTOR pathway in mice. Inflammation 46: 1531-1542, 2023.
31. Ferrara N, Gerber HP and LeCouter J: The biology of VEGF and its receptors. Nat Med 9: 669-676, 2003.
32. Tomuleasa C, Tigu AB, Munteanu R, Moldovan CS, Kegyes D, Onaciu A, Gulei D, Ghiaur G, Einsele H and Croce CM: Therapeutic advances of targeting receptor tyrosine kinases in cancer. Signal Transduct Target Ther 9: 201, 2024.
33. Peuget S, Zhou X and Selivanova G: Translating p53-based therapies for cancer into the clinic. Nat Rev Cancer 24: 192-215, 2024.
34. Tuval A, Strandgren C, Heldin A, Palomar-Siles M and Wiman KG: Pharmacological reactivation of p53 in the era of precision anticancer medicine. Nat Rev Clin Oncol 21: 106-120, 2024.
35. Rodriguez Calleja L, Lavaud M, Tesfaye R, Brounais-Le-Royer B, Baud'huin M, Georges S, Lamoureux F, Verrecchia F and Ory B: The p53 family members p63 and p73 roles in the metastatic dissemination: Interactions with microRNAs and TGFβ pathway. Cancers (Basel) 14: 5948, 2022.
36. Sampath D, Calin GA, Puduvalli VK, Gopisetty G, Taccioli C, Liu CG, Ewald B, Liu C, Keating MJ and Plunkett W: Specific activation of microRNA106b enables the p73 apoptotic response in chronic lymphocytic leukemia by targeting the ubiquitin ligase Itch for degradation. Blood 113: 3744-3753, 2009.
37. Humbert M, Federzoni EA and Tschan MP: Distinct TP73-DAPK2-ATG5 pathway involvement in ATO-mediated cell death versus ATRA-mediated autophagy responses in APL. J Leukoc Biol 102: 1357-1370, 2017.
38. Browne IM, André F, Chandarlapaty S, Carey LA and Turner NC: Optimal targeting of PI3K-AKT and mTOR in advanced oestrogen receptor-positive breast cancer. Lancet Oncol 25: e139-e151, 2024.
39. Zhu L, Li XX, Shi L, Wu J, Qian JY, Xia TS, Zhou WB, Sun X, Zhou XJ, Wei JF and Ding Q: Rapamycin enhances the sensitivity of ER-positive breast cancer cells to tamoxifen by upregulating p73 expression. Oncol Rep 41: 455-464, 2019.
40. Lu Z, Jiao D, Qiao J, Yang S, Yan M, Cui S and Liu Z: Restin suppressed epithelial-mesenchymal transition and tumor metastasis in breast cancer cells through upregulating mir-200a/b expression via association with p73. Mol Cancer 14: 102, 2015.
41. Goossens S, Vandamme N, Van Vlierberghe P and Berx G: EMT transcription factors in cancer development re-evaluated: Beyond EMT and MET. Biochim Biophys Acta Rev Cancer 1868: 584-591, 2017.
42. Garinet S, Didelot A, Denize T, Perrier A, Beinse G, Leclere JB, Oudart JB, Gibault L, Badoual C, Le Pimpec-Barthes F, *et al*: Clinical assessment of the miR-34, miR-200, ZEB1 and SNAIL EMT regulation hub underlines the differential prognostic value of EMT miRs to drive mesenchymal transition and prognosis in resected NSCLC. Br J Cancer 125: 1544-1551, 2021.
43. Capdevila J, Carrato A, Tabernero J and Grande E: What could Nintedanib (BIBF 1120), a triple inhibitor of VEGFR, PDGFR, and FGFR, add to the current treatment options for patients with metastatic colorectal cancer? Crit Rev Oncol Hematol 92: 83-106, 2014.
44. Khalique S and Banerjee S: Nintedanib in ovarian cancer. Expert Opin Investig Drugs 26: 1073-1081, 2017.
45. Roth GJ, Binder R, Colbatzky F, Dallinger C, Schlenker-Herceg R, Hilberg F, Wollin SL and Kaiser R: Nintedanib: From discovery to the clinic. J Med Chem 58: 1053-1063, 2015.
46. Tu J, Xu H, Ma L, Li C, Qin W, Chen X, Yi M, Sun L, Liu B and Yuan X: Nintedanib enhances the efficacy of PD-L1 blockade by upregulating MHC-I and PD-L1 expression in tumor cells. Theranostics 12: 747-766, 2022.
47. Mukhopadhyay B, Singh S and Singh A: Utilizing nanomaterials for cancer treatment and diagnosis: An overview. Discov Nano 19: 215, 2024.